

The role of tap duration for the steady state density of vibrated granular media

JOSHUA A. DIJKSMAN¹ and MARTIN VAN HECKE¹

¹ *Kamerlingh Onnes Lab, Universiteit Leiden, Postbus 9504, 2300 RA Leiden, The Netherlands*

PACS 45.70.-n –

PACS 45.70.Cc –

PACS 81.20.Ev –

Abstract. - We revisit the problem of compaction of a column of granular matter exposed to discrete taps. We accurately control the vertical motion of the column, which allows us to vary the duration T and the amplitude A of single-cycle sinusoidal taps independently. We find that the density of the material at the reversible branch depends both on A and T . By comparing the densities on the reversible branches obtained for a range of values of T , we find that we can collapse all data when plotted as function of A/T , which scales similar to both the liftoff velocity and the time of flight of the packing. We further show that switching between states obtained for different A and T , but chosen such that their densities on the reversible branches match, does not lead to appreciable hysteresis. We conclude that the appropriate control parameter for sinusoidal tapping is not the peak acceleration $\Gamma \sim A/T^2$, as is usually assumed, but rather $\Gamma T \sim A/T$.

Everyday experience tells us that granular materials compact when vibrated — think of tapping a tin of coffee powder in a can. Early experiments in the 1950s indicated that tapping can induce both dilation and compaction of a packing of granular materials, depending on the details of the tap [1]. More than a decade ago, a series of experiments probed the compaction of dry granular materials (glass beads) in a narrow tall tube which was tapped vertically [2–4]. Starting from a loose packing, the density was observed to exhibit slow, logarithmic growth as a function of the number of applied taps. Memory effects, in which the density evolution depended on the tapping history, were also found [5].

Eventually however, in all experiments a state was reached where the packing density depends only on the tapping strength and not on the history [6]. From such a state the so-called reversible branch could then be obtained repeatedly and reversibly by slowly ramping up and down the tapping intensity. The transient phenomena and memory effects all occur along the so called irreversible branch, along which the system would evolve before reaching the reversible branch.

In later studies of compaction in much wider containers, convection was found to be important [7–9]. In these experiments the temporal evolution of the density on the irreversible branch was found to be different [6–9], but

again the same reversible branch was found.

Here we address the following question: What is the appropriate control parameter that characterizes the taps? A widely used characterization of taps is the ratio of their peak acceleration and the gravitational acceleration, Γ . Certainly the peak acceleration is important in that it allows to distinguish between tap strengths where no liftoff of the packing occurs, for $\Gamma < \Gamma^* \approx 1$, and taps where that does happen [7]. Recent numerical work on the irreversible branch dynamics of compaction has suggested that the dimensionless acceleration parameter is not appropriate for rescaling the data [10]. Moreover, recent numerics [11] of compaction under sinusoidal driving vibrations indicate that the vibration frequency also influences the reversible branch, and similarly, supporting evidence for the role of tap duration can already be found in the observations of Macrae *et al.* [1].

Here we address the question of the appropriate control parameter experimentally, by studying the packing density on the reversible branch in experiments in which we expose granular packings to single cycle sinusoidal discrete taps with $\Gamma > 1$, where we control and vary both the tap amplitude A and its duration T (Fig. 1). For sinusoidal taps as used here, Γ can be given in terms of A and T : $\Gamma = A\omega^2/g$, with $\omega = 2\pi/T$ the radial frequency, and g the gravitational acceleration. Since we have precise con-

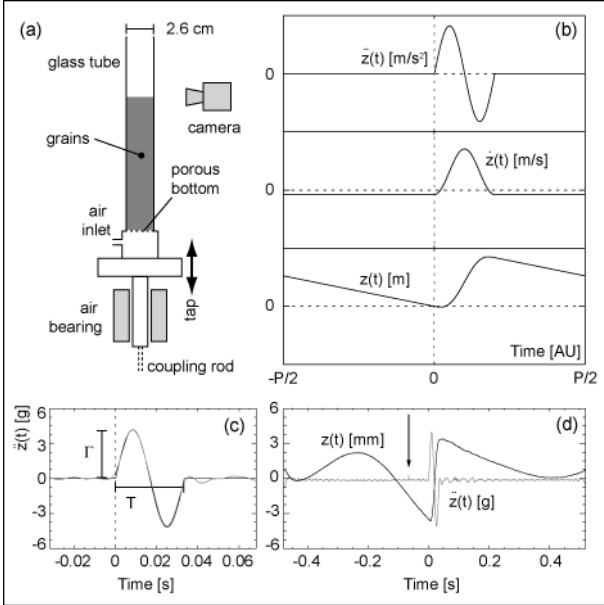


Fig. 1: (a) Sketch of the experimental setup. (b) Sketch of the waveforms of $\ddot{z}(t)$, $\dot{z}(t)$ and $z(t)$, illustrating the offset and linear slopes present in $z(t)$, stemming from continuity requirements. (c) Comparison between desired waveform (grey) and actual waveform (black) of the vertical acceleration $\ddot{z}(t)$. (d) A typical measured position (black) and acceleration (grey) signal. The arrow indicates the phase at which the packing fraction is measured.

trol over the acceleration signal, we can vary both Γ and ω independently (see Fig. 1b).

For given T , we obtain similar reversible branches $\phi_{\text{rev}}(\Gamma, T)$ as were observed before for fixed T , both for a bidisperse glass bead mixture and a bronze powder, and the reversible densities $\phi_{\text{rev}}(\Gamma, T)$ depend both on T and Γ . We find that all data can be collapsed in good approximation by plotting the packing fraction as function of ΓT , which is close to the liftoff velocity, or similarly, the time of flight of the granular packing. In addition we probe what happens when we alternate the taps between pairs of different Γ and T for which $\phi_{\text{rev}}(\Gamma, T)$ are equal, and we find no appreciable hysteresis.

The evidence that we will detail below will show that Γ is not the appropriate control parameter for compaction. Our results suggest that the density of the reversible branch is controlled by the product of Γ and large T . Hence, by maximizing ΓT instead of Γ , a wider range of agitation strengths can be reached.

Experimental Methods. — *Setup.* We study granular compaction in a glass tube (diameter 26 mm, height 20 cm) filled with grains (typical filling height 10 cm). The glass tube is shaken vertically with a shaker (VG100, VTS systems), driven by a commercial audio amplifier (Crown CE1000). The vertical motion of the tube is guided by an air bearing ($\varnothing 1''$, New Way) which is levelled. Levelling eliminates heaping, the unwanted tilting of the surface of

granular media subjected to vibrations [12]. An 0.5 meter long and flexible aluminum rod couples the tube and the shaker (see Fig. 1a). This rod eliminates the necessity of excessively accurate alignment of the axes of the air bearing and the shaker.

The vertical acceleration of the tube is measured with an accuracy of $10^{-3}g$, by a combination of two accelerometers (Dytran E3120AK and a modified ADXL320EB). For consistency checks, we occasionally monitor the position $z(t)$ of the glass tube with an inductive position sensor (Messotron WLH50, $10^{-5}m$ resolution) — the acceleration measurements are far more sensitive and these will be used in the feedback scheme described below.

Tap — In order to create a tap where both the duration and strength can be controlled independently, we need to determine the waveform $z(t)$. We denote the duration of the tap by $T = 2\pi/\omega$, the period of the tap by P (we will fix it later at 1 second), and have the tap start at $t = 0$. We demand that that $z(t)$, $\dot{z}(t)$ and $\ddot{z}(t)$ are continuous, that $\int dt \dot{z}(t) = 0$ and $\int dt \ddot{z}(t) = 0$, and that $z(0) = 0$. These requirements severely constrain the tap — for example, taking for $z(t)$ a single sine cycle followed by a period where $z = 0$ makes $\ddot{z}(t)$ discontinuous. Starting from a single sine cycle for $\ddot{z}(t)$, obtaining $\dot{z}(t)$ and $z(t)$ by integration, and fixing the integration constants so that the continuity conditions are full filled, we find the waveform summarized in Table 1 (see Fig. 1b):

	$0 \leq t \leq T$	$T \leq t \leq P$
\ddot{z}	$A\omega^2 \sin(\omega t)$	0
\dot{z}	$-A\omega \cos(\omega t) + b_1$	$-b_2$
z	$-A \sin(\omega t) + b_1 t$	$-b_2(t - P)$

Table 1: Waveform of the tap. Here the integration constants equal $b_1 = A\omega(P - T)/P$ and $b_2 = a\omega T/P$.

In order to create such a tap, a feedback algorithm is used to adapt the Fourier components of the signal fed into the audio amplifier such that the measured acceleration signal converges to the desired waveform. This procedure is carried out once, before the start of the experiment, and the shape of the output wave is not changed during the actual experiment; it is only multiplied by a scale factor to set its overall amplitude. We have checked that the system is sufficiently linear so that re-calibration of the waveform is not necessary when Γ is varied.

Taps are applied once every second, so $P = 1$; this allows the packing to come completely to rest before the start of a new tap. In Fig. 1c, the desired waveform for $\ddot{z}(t)$ is compared to a typical measured acceleration signal — the waveform produced by the feedback scheme is in good agreement with the desired tap. In Fig. 1d, a measured waveform for $z(t)$ and accompanying $\ddot{z}(t)$ are shown. The slow downward motion of the tube anticipated in Table 1 is clearly visible. This downward motion is not at constant speed due to low-frequency limitations in the electronics

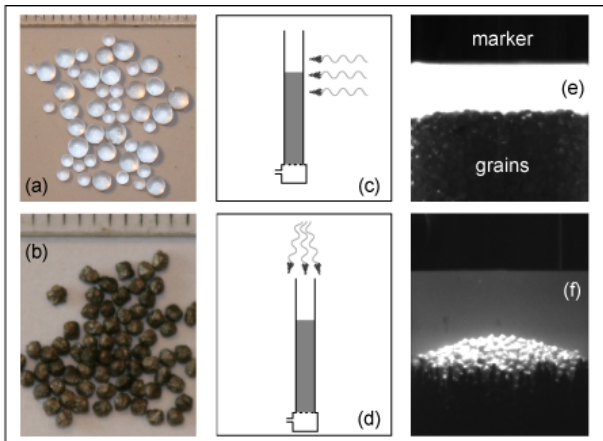


Fig. 2: (Color online) The granular material used in the experiment (scale = 1mm): (a) glass beads, (b) bronze powder. Illumination direction: (c) for glass, from the back, (d) for bronze, from the top. Typical camera image (e) glass, (f) bronze. For bronze powder two cameras are used, image is typical for both.

that drive the shaker. The accelerations associated with this non-constant speed are however always below g , so they do not influence the packing fraction measurably.

Parameter Range and Grain Dynamics. As was established in [7], the dynamics of compaction dramatically slows down when the tapping peak acceleration Γ falls below a critical value Γ^* which is typically slightly above 1. This transition is accompanied by a change from a regime where the grains experience lift off for $\Gamma > \Gamma^*$ to a regime where they do not. In our experiments, the values of Γ range from 1 to 15, and by high speed imaging we have established a clear lift off and expansion of the whole column of grains for $\Gamma \gtrsim 2$ — the precise value of Γ^* in our experiments is likely somewhat smaller. The vast majority of our data is therefore taken in the regime where the grains loose contact with the bottom plate and their neighbors.

Packing Density and Material Used. The packing density is determined from the height of the granular column, and this height is measured with a camera that observes the packing from the side, as in Refs. [13, 14]. The camera is triggered for strobed image acquisition, such that the camera takes a picture just before the start of the tap: the trigger moment is indicated by the arrow in Fig. 1d. A ring-shaped dark marker, whose height from the bottom of the tube is known (typically 13 cm), is attached to the tube, slightly above the maximum height of the bead pack. Depending on the grains used we use lighting from behind (for glass beads), or from the top (for bronze powder) — see Fig. 2. Determining the height of the packing in both cases amounts to counting pixels with intensity above a certain threshold value. The threshold value is determined from the histogram of a typical image. We verified that the imaging method applied gives a linear relationship between the amount of

grains in the tube and the number of pixels in the gap.

We employ two types of granular matter: a bidisperse mixture of glass beads (Pneumix, 1.6 and 2.3 mm in 1:1 volume mixture, Fig. 2a), or monodisperse bronze powder (Acupowder, grade '12HP', ~ 1 mm diameter, Fig. 2b). Due to their different opacity, optimal lighting is different for these materials (Fig. 2c-d). One more difference is that glass bead packings generally have a flat surface, while the bronze beads grow a small radially symmetric heap at their surface (this heap is likely due to convection). One important difference is that the glass beads tend to be more sensitive to triboelectric effects, which result in overall, run-to-run variations of the absolute density (the trends in the variation of ϕ_{rev} with Γ are not affected by such variations). We observe that such variations are absent for the bronze powder. Importantly, our essential findings (control parameter $\sim \Gamma T$ and no hysteresis) are seen with both materials.

Our measurement method yields a high resolution; the noise in the determination of the height in the packing due to camera pixel noise alone is $30\mu\text{m}$, this translates into a variation of ϕ of $\sim 0.03\%$. However, this method gives a relatively poor accuracy in the absolute value of ϕ . This is due to the cumulative effect of the errors in the determination of the height of the marker, the inner diameter of the tube, the density of the beads, image calibration and the thresholding. The packing fractions stated in this paper therefore have an estimated systematic error of 1.2%.

Experimental Protocol. The bottom of the tube is perforated and connected to a flow box so dry air can be pumped through the bead pack. We always start an experiment by fluidizing the packing with several pulses of dried compressed air. This procedure creates an initial packing density of order 0.60 ± 0.01 . The number of flow pulses is generally not the same for each experiment; several pulses are applied initially to ensure a proper erasure of memory effects [2, 14], after which pulses are applied until a packing with a flat surface is obtained. Airflow is turned off during all compaction experiments, which simply consist of observing how ϕ evolves while taps are applied.

Transients & Steady State. — Fig. 3a shows how the packing typically changes with the number of taps applied to the system, in an experiment where a packing of glass beads is subjected to 250000 taps with $T = 33$ ms, and where the amplitude is altered between $\Gamma \sim 2$ and $\Gamma \sim 6$ after each 25000 taps. The packing fraction is only measured every 10 taps. There are several distinct features in this graph: (i) *Initial transient:* Initially the packing fraction evolves slowly towards a steady state value, nonmonotonically in the case depicted in Fig. 3b. (ii) *Steady state:* After the transient the system is able to reach a steady state packing fraction. The correspondence between ϕ and Γ is also reproducible: changing tap

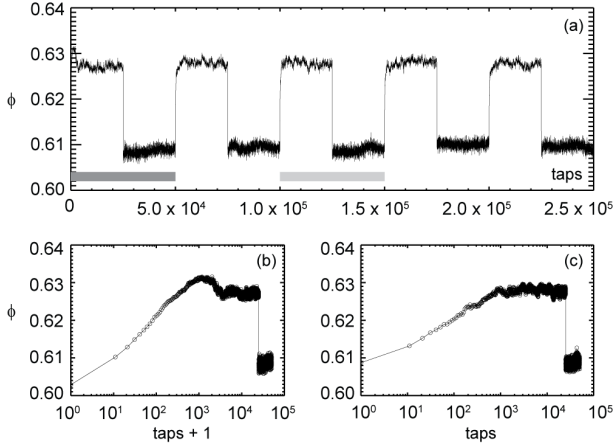


Fig. 3: (a) Evolution of the packing fraction as function of the number of taps. Here, we fix $T = 33$ ms, and Γ is alternated between $\Gamma = 2$ and $\Gamma = 6$ every 25000 taps. Our data shows that after a short transient, the density can be reversibly changed from one value to another. (b) The initial transient compaction behavior on a logarithmic scale, for the range indicated by the dark grey bar in panel (a). (c) A typical compaction process between two steady states as occurs at $t = 10^5$ as indicated by the light grey bar in panel (a).

amplitudes repeatedly back and forth shows that for a particular tap amplitude the same steady state packing fraction is always obtained (Fig. 3a). (iii) *Amplitude step transient*: When the amplitude of the tap changes, the packing fraction changes too, but not instantaneously. This time dependent process is usually not symmetric in the step direction: an increase of the tap amplitude usually almost immediately dilates the packing to the packing fraction appropriate for the new amplitude. A step down in tap amplitude requires compaction of the packing to reach the steady state packing fraction belonging to the lower tap amplitude. This process is usually slower. As can be seen in Fig. 3c, the increase in density from roughly 0.61 to the plateau value ≈ 0.63 takes of the order of 1000 taps, comparable to the initial transient duration.

The initial transient is somewhat different in each experiment, and run-to-run fluctuations of details of $\phi(t)$ are considerable. For example, non-monotonicity seen in $\phi(t)$ in Fig. 3 is not always observed. This may either be due to the fact that the preparation of the packing in each experiment is slightly different, or to inherent fluctuations of the density evolution. We identify the transient behavior with the irreversible branch, and the steady state with the reversible branch.

The strength of the fluctuations in the early evolution in $\phi(t)$ hinder a precise comparison of our results to the results from the Chicago and Rennes groups [2,3,9]. However, our values for the densities on the reversible branch, $\phi_{\text{rev}}(\Gamma)$, are far more robust, and in the rest of the paper we focus on $\phi_{\text{rev}}(\Gamma, T)$ in the steady state.

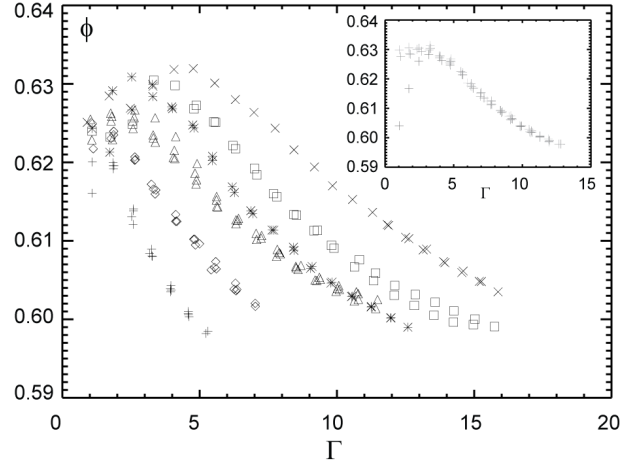


Fig. 4: Reversible and irreversible branch for the glass bead mixture (See text). The main panel shows the reversible branch $\phi_{\text{rev}}(\Gamma, T)$ for different tap lengths T (+ 50ms, \diamond 33ms, \triangle 16ms, $*$ 14ms, \square 13ms, \times 10ms). Clearly Γ alone is not sufficient to characterize the tapping. The inset shows $\phi_{\text{rev}}(\Gamma, T)$ for $T=14.3$ ms, and four sweeps in Γ (see text). Greyscale of symbols indicates measurement time; lighter points are later measurements. After an initial transient (black crosses), the densities become history independent.

Steady-State Density as a Function of Γ and T . — As we will show, our experimental protocol allows the determination of $\phi_{\text{rev}}(\Gamma, T)$. At fixed T , this enables use to reproduce the reversible and irreversible branch in a $\phi_{\text{rev}}(\Gamma, T)$ -plot similar to those found before in the Chicago and Rennes experiments by sweeping Γ up and down several times.

In the inset of Fig. 4 we show that the packing density becomes well-defined on the reversible branch. In this experiment, starting from a low density packing, the tap amplitude is swept up and down four times, and the number of taps at each different tap amplitude is 4000. Every 20 taps the packing fraction is measured and each data point corresponds to an average over the resulting 200 measurements. The irreversible branch is visible as the initial increase of ϕ with Γ . After about 12,000 taps the reversible branch is reached: this branch is clearly shown in the four amplitude sweeps that all follow the same $\phi_{\text{rev}}(\Gamma, T)$ relation, with ϕ_{rev} decreasing with Γ .

Effect of the tap duration. We will now explore the reversible branch for a range of values of T (Fig. 4). The reversible branches obtained in a series of experiments in which Γ is swept for a range of values of T are shown in the main panel of Fig. 4. The reversible branches for different tap lengths T clearly have the same overall form, but do not coincide — Γ alone is not the parameter that governs compaction. The spacing of the data and the fact that the functional form of $\phi_{\text{rev}}(\Gamma, T)$ is similar for different T , strongly suggests the data sets can be collapsed onto a master curve. Fig. 5 shows that $\phi_{\text{ref}}(\Gamma, T)$ can be

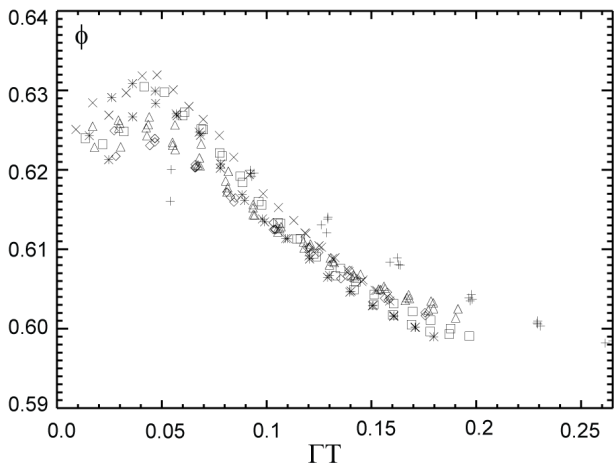


Fig. 5: Data for the reversible branches for the glass bead mixture as shown in Fig. 4 can be collapsed well when plotted as function of ΓT .

collapsed reasonably well by plotting ϕ_{rev} as a function of the product ΓT .

Bronze powder. For the bronze powder, we measured the reversible branch $\phi_{\text{rev}}(\Gamma, T)$ for different values of the tap length T ; the results are shown in the inset of Fig. 6. Note that the range of packing fractions obtained is far larger for the bronze powder, which may be attributed to the roughness of the particles [15]. Similarly to the glass beads, ϕ_{rev} collapses onto a master curve when plotted as function of ΓT — see Fig. 6. This shows that the details of the granular material used are entirely insignificant.

Absence of hysteresis. In Ref. [5] memory effects were observed in the evolution of the packing fraction on the irreversible branch: two different initial conditions were prepared at a certain fixed ϕ , by compacting low density systems at different tapping strength. The time evolution of subsequent compaction differed, despite the fact that the initial packing fraction and tap strength were equal — hence not only the packing fraction, but also the history is important for the evolution at the irreversible branch.

While such memory effects have not been seen, per definition, on the reversible branch, one may wonder if some more subtle hysteretic effects could arise there. In particular, if the state of the system on the reversible branch is not fully specified by density, it might be that using two control parameters, subtle hysteretic effects not seen when only sweeping the single parameter Γ become apparent.

Since data for ϕ_{rev} as a function of Γ and T can be collapsed on a single master curve, it follows that Γ and T can be varied at the same time in such a way that ϕ_{rev} stays constant. As we will show, we do not observe any appreciable hysteretic effects when switching between different pairs of (Γ, T) adjusted so that $\phi_{\text{rev}}(\Gamma, T)$ is constant.

We measure the packing fraction of a bronze powder packing while we expose the granular packing to taps with a sequence of different T : 17,33,17,11 ms (Fig. 7a) and different Γ . This sequence is repeated three times; each

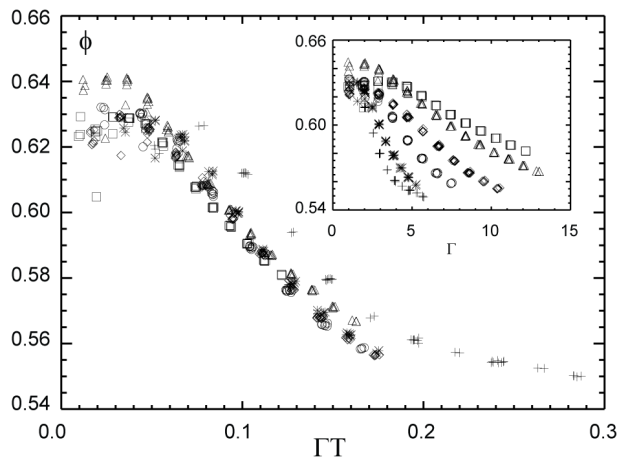


Fig. 6: $\phi_{\text{rev}}(\Gamma T)$ for the rough bronze powder. Symbols: + 50ms, * 33ms, \circ 22ms, \diamond 17ms, \triangle 13ms, \square 10ms. Inset: Same data, $\phi_{\text{rev}}(\Gamma, T)$ for the different T .

Γ, T -pair was used for 10000 taps, the total number of taps applied in the experiment is 130000. The amplitude Γ (4.84, 2.88, 4.84, 7.32) for each different T , shown in Fig. 7b, was fine tuned such that the resulting packing fraction stayed the same during the whole experiment; the product ΓT is constant to within 10%. This 10% variation suggests that ΓT is likely an effective approximation of the ultimate order parameter that sets the density on the reversible branch — see below. The packing fraction evolution during the experiment is shown in Fig. 7c. No appreciable transients are observed when switching Γ and T : there is no evidence for any appreciable hysteresis. Our data is further evidence that memory effects, which are a characteristic of the irreversible branch, do not play a role on the reversible branch.

Interpretation. — How can we understand the relevance of ΓT in determining ϕ_{rev} ? We note that the liftoff velocity \dot{z}_l , the time-of-flight τ_f and impact velocity \dot{z}_i are all approximately, although not precisely, proportional to ΓT . Below we briefly discuss these parameters, but note already here that the experimental scatter prevents us from unambiguously determining whether these provide better scaling collapse than the simple ΓT scaling employed above.

(i) *Liftoff velocity* — The liftoff velocity \dot{z}_l is determined by calculating the velocity at the time where the acceleration falls below a threshold $-g\Gamma^*$. In case the packing experiences no friction with the container walls, this threshold equals the gravitational acceleration ($\Gamma^* = 1$), but in general Γ^* is somewhat larger, typically around 1.2. For given Γ^* and waveforms as described above, one finds that in the parameter regime where liftoff occurs ($\Gamma > \Gamma^*$), the liftoff velocity is given by

$$\dot{z}_l = \Gamma T \times \left(\frac{g}{2\pi} \left[1 + \sqrt{1 - (\Gamma^*/\Gamma)^2} - \frac{T}{P} \right] \right). \quad (1)$$

For most parameter values, the term within square brack-

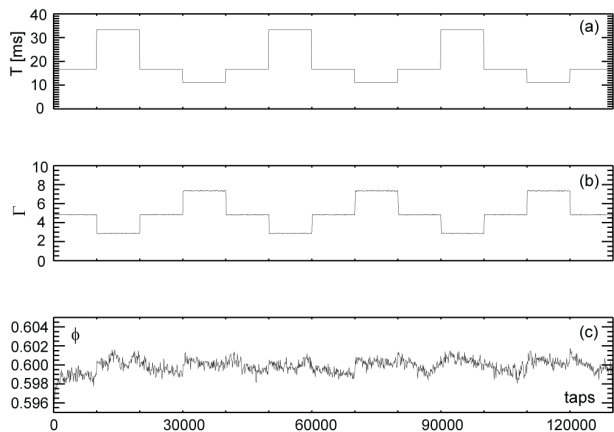


Fig. 7: T (a) and Γ (b) used in the constant packing fraction sweep. The packing fraction evolution in time is shown in (c); the fluctuations visible in (c) are of the order of the experimental noise. For details see text.

ets is close to two — typically, T/P is of order of a few percent, and for $\Gamma > 5$, the square root term is within a few percent equal to one. The main deviations between the scaling of ΓT and \dot{z}_l occur for small Γ . Our scatter is relatively large in this regime, and in a plot of ϕ_{rev} as function of \dot{z}_l , the quality of the collapse is very similar to when ΓT is used.

(ii) *Time of flight* — In rough approximation, the time of flight τ_f is simply proportional to the liftoff velocity: $\tau_f = 2\dot{z}_l/g$. We have also calculated the time of flight numerically, assuming either the analytic expressions for $z(t)$ and $\ddot{z}(t)$, or using the experimental data available for $z(t)$ and $\ddot{z}(t)$, and taking drag forces into account (these affect the total time of flight of the packing [16]). Despite the presence of free fit parameters (take-off acceleration, drag coefficient), the resulting data collapse when τ_f is used as scaling parameter is only marginal better than for ΓT or \dot{z}_l .

(iii) *Impact velocity* — The amount of energy dissipated once the packing comes to rest in the container is set by the impact velocity, and this could also be an appropriate choice of rescaling parameter. However, in the range of parameters explored, the impact velocity scales very similar to the time of flight, and the quality of the collapse does not improve.

We hence conclude that while impact velocity or time of flight might give a marginal improvement in the data collapse, the much simpler rescaling parameter ΓT works essentially equally well.

Conclusions. — By precisely controlling the shape of the taps, we find that the compaction of vibrated granular media is not only governed by Γ , the dimensionless peak acceleration, but that the tap duration plays an equally important role. We observe a collapse of the reversible branch with ΓT , for two different types of granular materials. We do not see any evidence for hysteretic effects

when switching between different driving parameters that correspond to the same reversible-branch-density.

The time of flight, the liftoff velocity and the impact velocity all scale similar to ΓT , which makes it impossible to experimentally determine which parameter leads to the best data collapse. In experiments focussing on the transients in granular compaction [10], or on the hydrodynamic phases in vibrofluidize granular materials [17], the order parameter found was always proportional to the injected energy per vibration cycle. We suggest that our scaling supports the view that the energy injected is also the driving mechanism in compaction experiments.

The authors like to thank Jeroen Mesman for technical assistance. J.A.D. acknowledges support from the Dutch physics foundation FOM, and M. v. H. acknowledges support from NWO/VIDI.

REFERENCES

- [1] MACRAE J., FINLAYSON P.C. and GRAY W., *Nature*, **179** (1957) 1356.
- [2] KNIGHT J. B., FANDRICH C. G., LAU C. N., JAEGER H. M. and NAGEL S. R., *Phys. Rev. E*, **51** (1995) 3957.
- [3] NOWAK E. R., KNIGHT J. B., POVINELLI M. L., JAEGER H. M. and NAGEL S. R., *Powder Technology*, **94** (1997) 79.
- [4] BEN-NAIM E., KNIGHT J. B., NOWAK E. R., JAEGER H. M. and NAGEL S. R., *Physica D*, **123** (1998) 380.
- [5] JOSSERAND C., TKACHENKO A. V., MUETH D. M. and JAEGER H. M., *Phys. Rev. Lett.*, **85** (2000) 3632.
- [6] RICHARD P., NICODEMI M., DELANNEY R., RIBIÉRE P. and BIDEAU D., *Nature Mat.*, **4** (2005) 121.
- [7] PHILIPPE P. and BIDEAU D., *Phys. Rev. Lett.*, **91** (2003) 104302.
- [8] RICHARD P., PHILIPPE P., BARBE F., BOURLÈS S., THIBAUT X. and BIDEAU D., *Phys. Rev. E*, **68** (2003) 020301.
- [9] PHILIPPE P. and BIDEAU D., *EPL (Europhys. Lett.)*, **60** (2002) 677.
- [10] LUDEWIG F., DORBOLO S., GILET T. and VANDEWALLE T., *Eur. Phys. Lett.*, **84** (2008) 44001.
- [11] AN X., YANG R., ZOU R. and YU A., *Powder Technology*, **188** (2008) 102.
- [12] PAK H. K., VAN DOORN E. and BEHRINGER R. P., *Phys. Rev. Lett.*, **74** (1995) 4643.
- [13] SCHRÖTER M., GOLDMAN D. I. and SWINNEY H. L., *Phys. Rev. E*, **71** (2005) 030301.
- [14] DIVOUX T., GAYVALLET H. and GEMINARD J.-C., *Phys. Rev. Lett.*, **101** (2008) 148303.
- [15] AN X. Z., YANG R. Y., DONG K. J., ZOU R. P. and YU A. B., *Phys. Rev. Lett.*, **95** (2005) 205502.
- [16] LUMAY G. and VANDEWALLE N., *Phys. Rev. E*, **74** (2006) 021301.
- [17] ESHUIS P., VAN DER WEELE K., VAN DER MEER D. and LOHSE D., *Phys. Rev. Lett.*, **95** (2005) 258001.